

Efficient Signed Graph Sampling via Balancing & Gershgorin Disc Perfect Alignment

Chinthaka Dinesh, *Member, IEEE*, Gene Cheung, *Fellow, IEEE*, Saghar Bagheri, *Student Member, IEEE*, and Ivan V. Bajić, *Senior Member, IEEE*

Abstract—A basic premise in graph signal processing (GSP) is that a graph encoding pairwise (anti-)correlations of the targeted signal as edge weights is exploited for graph filtering. However, existing fast graph sampling schemes are designed and tested only for positive graphs describing positive correlations. In this paper, we show that for datasets with strong inherent anti-correlations, a suitable graph contains both positive and negative edge weights. In response, we propose a linear-time signed graph sampling method centered on the concept of balanced signed graphs. Specifically, given an empirical covariance data matrix $\bar{\mathbf{C}}$, we first learn a sparse inverse matrix (graph Laplacian) \mathcal{L} corresponding to a signed graph \mathcal{G} . We define the eigenvectors of Laplacian \mathcal{L}_B for a balanced signed graph \mathcal{G}_B —approximating \mathcal{G} via edge weight augmentation—as graph frequency components. Next, we choose samples to minimize the low-pass filter reconstruction error in two steps. We first align all Gershgorin disc left-ends of Laplacian \mathcal{L}_B at smallest eigenvalue $\lambda_{\min}(\mathcal{L}_B)$ via similarity transform $\mathcal{L}_p = \mathbf{S}\mathcal{L}_B\mathbf{S}^{-1}$, leveraging a recent linear algebra theorem called Gershgorin disc perfect alignment (GDPA). We then perform sampling on \mathcal{L}_p using a previous fast Gershgorin disc alignment sampling (GDAS) scheme. Experimental results show that our signed graph sampling method outperformed existing fast sampling schemes noticeably on various datasets.

Index Terms—Graph signal processing, graph spectrum, graph sampling, Gershgorin circle theorem.

I. INTRODUCTION

A central premise in *graph signal processing* (GSP) [1], [2]—a growing field studying discrete signals on combinatorial graphs—is that a graph captures inter-node (anti-)correlations in the data as edge weights. Given a graph encoded with pairwise signal statistics, a myriad of processing tasks exploit the available graph kernel via graph filtering: compression, denoising, dequantization, etc [3]–[5]. In particular, *graph sampling*¹ [6] addresses the problem of choosing a subset of nodes to collect samples, so that the entire signal can be reconstructed in high fidelity under a signal smoothness / bandlimited assumption. Among many methods in the graph sampling literature are fast *eigen-decomposition-free* (EDF) schemes that mitigate full computation of frequency-defining eigenvectors of large graph Laplacian matrices [7]–[10]. Various mathematical tools were employed to realize the EDF

Chinthaka Dinesh, Gene Cheung, and Saghar Bagheri are with the Department of Electrical Engineering & Computer Science, York University, Toronto, Canada, e-mail: {dineshc, genec, sagharb}@yorku.ca.

Ivan V. Bajić is with the School of Engineering Science, Simon Fraser University, Burnaby, BC, Canada, e-mail: ibajic@ensc.sfu.ca.

Gene Cheung acknowledges the support of the NSERC grants RGPIN-2019-06271, RGPAS-2019-00110.

¹Graph sampling can be divided into aggregation sampling, local measurements, and node subset selection. We focus on the last category here.

property: spectral proxies (SP) [7], Neumann series (NS) [8], localization operator (LO) [9], and Gershgorin disc alignment (GDA) [10]. Common among these EDF methods is that they are designed and tested only for *positive* graphs capturing positive inter-node correlations.

However, there exist practical real-world datasets with strong inherent *anti-correlations*. For example, voting records in the Canadian Parliament often show opposing positions between the left-leaning Liberal and right-leaning Conservative parties². For such datasets, a most suitable graph kernel is instead a *signed* graph with both positive and negative edge weights [11], [12]. In response, in this paper³ we propose a linear-time signed graph sampling method, the first in the graph sampling literature. The key concept in our work is a *balanced signed graph* [15]—a signed graph with no cycles of odd number of negative edges. We show that balanced signed graphs have a natural definition of graph frequencies, and are more amenable to efficient sampling than unbalanced graphs.

Our sampling method can be summarized as follows. Given an empirical covariance matrix $\bar{\mathbf{C}}$ computed from data, we first employ *graphical lasso* (GLASSO) [16] to learn a sparse inverse matrix \mathcal{L} , interpreted as generalized graph Laplacian to a signed graph \mathcal{G} . We argue that eigenvectors of Laplacian \mathcal{L}_B for a balanced graph \mathcal{G}_B approximating \mathcal{G} —via edge weight augmentation in linear time—can be defined as graph frequency components. Our graph frequency notion based on eigenvectors of generalized Laplacians has practical implications: solutions to *maximum a posteriori* (MAP) formulations regularized with graph smoothness priors [17] are interpretable *low-pass* (LP) filters—bias to signals with zero-crossings maximally consistent with graph edge signs.

Next, we choose samples to minimize the worst-case LP-filter signal reconstruction error. While previous graph sampling scheme *Gershgorin Disc Alignment Sampling* (GDAS) [10] has roughly linear-time complexity, it is applicable only if Gershgorin disc left-ends [18] are initially aligned. We thus leverage a recent linear algebra theorem called *Gershgorin Disc Perfect Alignment* (GDPA) [19]: disc left-ends of a generalized graph Laplacian \mathbf{M} for a balanced graph can be exactly aligned at the smallest eigenvalue $\lambda_{\min}(\mathbf{M})$ via a similarity transform $\mathbf{S}\mathbf{M}\mathbf{S}^{-1}$, where $\mathbf{S} = \text{diag}(v_1^{-1}, \dots, v_N^{-1})$ and $\mathbf{v} = [v_1 \dots v_N]^\top$ is the first eigenvector of \mathbf{M} . Given GDPA, we compute $\mathcal{L}_p = \mathbf{S}\mathcal{L}_B\mathbf{S}^{-1}$, so that disc left-ends

²<https://www.ourcommons.ca/members/en/votes>

³An earlier version of our sampling scheme [13], [14] targeted 3D point clouds specifically. We discuss sampling for general signals on signed graphs here.

of \mathcal{L}_p are perfectly aligned at $\lambda_{\min}(\mathcal{L}_B)$. Finally, we perform sampling on \mathcal{L}_p using GDAS. Experimental results show that our signed graph sampling method outperformed existing fast sampling schemes [7]–[10] on different datasets.

The paper outline is as follows. Related works and preliminaries are reviewed in Sections II and III, respectively. We present our frequency notion for balanced signed graphs in Section IV. We formulate an optimization problem to reconstruct a graph signal from samples in Section V, and present our signed graph sampling method in Sections VI and VII. Experimental results and conclusion are presented in Sections VIII and IX, respectively.

II. RELATED WORK

We first discuss related works in graph sampling, then review existing graph smoothness definitions in the literature.

A. Graph Sampling

There are three variants of the graph sampling problem: *aggregation sampling* [20], [21], *local weighted sampling* [22], and *node subset sampling* [7], [23]–[28]. In this paper, we focus only on the last one.

Existing node subset sampling methods in the literature can be divided into *deterministic* methods [7], [23]–[28] and *random* methods [27], [29]. Deterministic approaches select a subset of nodes so that a target cost function related to the signal reconstruction error is minimized. Random methods select nodes randomly according to a pre-determined probability distribution. Random sampling methods have lower computational complexity, but they typically require more samples for the same reconstruction quality compared to their deterministic competitors.

Most existing deterministic methods [7], [23]–[28] extended the notion of *Nyquist sampling* in regular data kernels—sparse representation of low-pass / smooth signals—to irregular kernels described by graphs, where graph frequencies are defined as eigenvectors of a 1-hop graph variation operator, such as graph Laplacian or adjacency matrix. [30], [31] chose samples greedily to minimize the minimum mean square error (MMSE) of signal reconstruction, also known as the *A-optimality criteria* [32]. Alternatively, [24] used the *E-optimality criteria*, which can be interpreted as minimizing the worst case MSE. [7] proposed a lightweight sampling method via *spectral proxy*, which obtained samples based on the first eigenvector of a Laplacian sub-matrix in each greedy step. However, all these methods [7], [24], [30], [31] required extreme eigen-pair computation of the graph variation operator or its sub-matrix to choose each sample, which is computationally complex and thus not scalable to larger graphs. Recently, [25] avoided eigenvector computation via Neumann series, but required a large number of matrix multiplications for accurate approximation, which is also expensive.

To avoid large computation cost, [9], [33] proposed an *eigen-decomposition-free* (EDF) graph sampling method by successively maximizing the coverage of the localization operators, based on Chebyshev polynomial approximation [34]. However, this method does not have any global error measure

in its optimization objective. Orthogonally, [10] proposed Gershgorin disc alignment sampling (GDAS) based on Gershgorin circle theorem (GCT) [18] without any explicit eigen-decomposition. We employ GDAS as the final step in our graph sampling strategy.

All the aforementioned graph sampling methods were designed for positive graphs without self-loops. Our early work [13], [14] proposed a deterministic graph sampling method for signed graphs exclusively for 3D point cloud subsampling. In this paper⁴, we propose a general frequency notion for balanced signed graphs based on eigenvectors of a generalized graph Laplacian matrix, resulting in a more interpretable LP filter system for signal reconstruction from samples via a MAP formulation with a graph smoothness prior [17].

B. Graph Smoothness Priors

Numerous graph smoothness priors—measure of smoothness of signal \mathbf{x} w.r.t. graph \mathcal{G} —have been proposed in the literature to regularize ill-posed signal restoration problems like denoising and interpolation [2]. The most common is the *graph Laplacian regularizer* (GLR) [17], $\mathbf{x}^\top \mathbf{L} \mathbf{x}$, where \mathbf{L} is a combinatorial graph Laplacian matrix specifying graph \mathcal{G} . Another is *graph shift variation* (GSV) [36], $\|(\mathbf{I} - \rho_{\max}^{-1} \mathbf{W})\mathbf{x}\|_2^2$, stating that signal \mathbf{x} and its shifted version $\rho_{\max}^{-1} \mathbf{W} \mathbf{x}$ (where adjacency matrix \mathbf{W} scaled by the inverse of the spectral radius ρ_{\max} is interpreted as a graph shift operator) should be similar, and thus their difference should induce a small ℓ_2 -norm. Other priors include *graph total variation* (GTV) [37], [38], *gradient graph Laplacian regularizer* (GGLR) [39], etc. These priors typically have associated *spectral* interpretations: a smooth signal is also a low-frequency signal in an appropriate graph spectrum. For example, in [40], graph frequencies are defined as eigen-pairs of a generic one-hop graph variation operator, such as combinatorial graph Laplacian matrix \mathbf{L} , normalized Laplacian matrix \mathcal{L} , random walk Laplacian matrix \mathbf{L}_{RW} , adjacency matrix \mathbf{W} , and random walk matrix \mathcal{Q} .

However, previous graph frequency definitions [34], [41]–[45] are restricted to the *positive* graphs *without self-loops*. In this paper, we extend this frequency notion to positive and balanced signed graphs with self-loops, based on eigenvectors of the *generalized graph Laplacian matrix* [46], which can be readily computed from data using empirical graph learning schemes like GLASSO [16].

III. PRELIMINARIES

We first review basic concepts in graph signal processing (GSP), Gershgorin Circle Theorem (GCT), and balanced signed graphs. We review derivation of the discrete cosine transform (DCT) in [47], which will lead to our definition of graph frequencies in Section IV. Finally, we review a popular precision matrix estimation algorithm (GLASSO) [16].

A. Definitions in Graph Signal Processing

1) *Graph Definitions*: A undirected weighted graph $\mathcal{G} = (\mathcal{V}, \mathcal{E}, \mathbf{W})$ is defined by a set of N nodes

⁴This is a journal version of our recent conference paper in [35].

$\mathcal{V} = \{1, \dots, N\}$, edges $\mathcal{E} = \{(i, j)\}$, and a symmetric *adjacency matrix* \mathbf{W} . $W_{i,j} \in \mathbb{R}$ is the edge weight if $(i, j) \in \mathcal{E}$, and $W_{i,j} = 0$ otherwise. Self-loops may exist, in which case $W_{i,i} \in \mathbb{R}$ is the weight of the self-loop for node i . Diagonal *degree matrix* \mathbf{D} has diagonal entries $D_{i,i} = \sum_j W_{i,j}, \forall i$. A *combinatorial graph Laplacian matrix* \mathbf{L} is defined as $\mathbf{L} \triangleq \mathbf{D} - \mathbf{W}$ [1]. If self-loops exist, then the *generalized graph Laplacian matrix* \mathcal{L} accounting for self-loops is $\mathcal{L} \triangleq \mathbf{D} - \mathbf{W} + \text{diag}(\mathbf{W})$ [46].

A graph signal $\mathbf{x} \in \mathbb{R}^N$ is “smooth” w.r.t. graph \mathcal{G} if its *graph Laplacian regularizer* (GLR), $\mathbf{x}^\top \mathcal{L} \mathbf{x}$, is small [4]:

$$\mathbf{x}^\top \mathcal{L} \mathbf{x} = \sum_{(i,j) \in \mathcal{E}} W_{i,j} (x_i - x_j)^2 + \sum_{i=1}^N W_{i,i} x_i^2. \quad (1)$$

GLR is a measure of signal variation over a defined graph \mathcal{G} specified by \mathcal{L} . It is used to regularize ill-posed restoration problems such as denoising and dequantization [4], [5].

2) *Graph Spectrum*: Given combinatorial \mathbf{L} is real and symmetric, one can diagonalize $\mathbf{L} = \mathbf{U} \mathbf{\Lambda} \mathbf{U}^\top$, where $\mathbf{\Lambda} = \text{diag}(\lambda_1, \dots, \lambda_N)$ is a diagonal matrix containing eigenvalues $\{\lambda_k\}_{k=1}^N$ along its diagonal, and \mathbf{U} contains corresponding eigenvectors $\{\mathbf{v}_k\}_{k=1}^N$ as columns. Common in the GSP literature [1], [2], the k -th eigen-pair $(\lambda_k, \mathbf{v}_k)$ is conventionally interpreted as the k -th graph frequency and Fourier mode. \mathbf{U}^\top is the *graph Fourier transform* (GFT) [1] that computes transform coefficients $\tilde{\mathbf{x}} = \mathbf{U}^\top \mathbf{x}$ of graph signal \mathbf{x} . Thus, one can express GLR for a positive graph without self-loops as

$$\mathbf{x}^\top \mathbf{L} \mathbf{x} = \mathbf{x}^\top \mathbf{U} \mathbf{\Lambda} \mathbf{U}^\top \mathbf{x} = \sum_{k=1}^N \lambda_k \tilde{x}_k^2. \quad (2)$$

A small GLR means that signal \mathbf{x} has most of its energy residing in low frequencies λ_k ’s, or \mathbf{x} is a *low-pass* (LP) signal. We extend the graph frequency notion for positive graphs to balanced *signed* graphs in Section IV.

B. Gershgorin Circle Theorem

Given a real symmetric matrix \mathbf{M} , corresponding to each row i is a *Gershgorin disc* i with center $c_i \triangleq M_{i,i}$ and radius $r_i \triangleq \sum_{j \neq i} |M_{i,j}|$. A corollary of *Gershgorin Circle Theorem* (GCT) [18] is that the smallest Gershgorin disc left-end $\lambda_{\min}^-(\mathbf{M})$ is a lower bound of the smallest eigenvalue $\lambda_{\min}(\mathbf{M})$ of \mathbf{M} , *i.e.*,

$$\lambda_{\min}^-(\mathbf{M}) \triangleq \min_i c_i - r_i \leq \lambda_{\min}(\mathbf{M}). \quad (3)$$

Note that a *similarity transform* $\mathbf{S} \mathbf{M} \mathbf{S}^{-1}$ for an invertible matrix \mathbf{S} has the same set of eigenvalues as \mathbf{M} . Thus, a GCT lower bound for $\mathbf{S} \mathbf{M} \mathbf{S}^{-1}$ is also a lower bound for \mathbf{M} , *i.e.*, for any invertible \mathbf{S} ,

$$\lambda_{\min}^-(\mathbf{S} \mathbf{M} \mathbf{S}^{-1}) \leq \lambda_{\min}(\mathbf{S} \mathbf{M} \mathbf{S}^{-1}) = \lambda_{\min}(\mathbf{M}). \quad (4)$$

C. Balanced Signed Graph

A *signed graph* is a graph with both positive and negative edge weights. The concept of balance in a signed graph was used in many scientific disciplines, such as psychology, social

networks and data mining [48]. In this paper, we adopt the following definition of a *balanced signed graph* [15], [19]:

Definition 1. A signed graph \mathcal{G} is balanced if \mathcal{G} does not contain any cycle with odd number of negative edges.

For intuition, consider a 3-node graph \mathcal{G} , shown in Fig. 1. Given the edge weight assignment in Fig. 1(left), we see that this graph is balanced; the only cycle has an even number of negative edges (two). Note that nodes can be grouped into two clusters—red cluster $\{i, k\}$ and blue cluster $\{j\}$ —where same-color node pairs are connected by positive edges, and different-color node pairs are connected by negative edges.

In contrast, the edge weight assignment in Fig. 1(right) produces a cycle of odd number of negative edges (one). This graph is not balanced. In this case, nodes cannot be assigned to two colors such that positive edges connect same-color node pairs, and negative edges connect different-color node pairs. Generalizing from this example, we state the well-known *Cartwright-Harary Theorem* (CHT) [15] as follows.

Theorem 1. A given signed graph is balanced if and only if its nodes can be colored into red and blue, such that a positive edge always connects nodes of the same color, and a negative edge always connects nodes of opposite colors.

Thus, to determine if a given graph \mathcal{G} is balanced, one can simply check if nodes can be colored into blue and red with *consistent* edge signs, as stated in Theorem 1, which can be done in linear time [19].

D. Discrete Cosine Transform

Variants of one-dimensional *Discrete Cosine Transform* (DCT) contain eigenvectors of a symmetric *second difference* matrix $\mathbf{T} \in \mathbb{R}^{N \times N}$, which is a tridiagonal matrix with diagonal elements 2 and sub- and super-diagonal elements -1 , except the first and last rows [47]:

$$\mathbf{T} = \begin{bmatrix} a & b & & & & & & \\ -1 & 2 & -1 & & & & & \\ & \ddots & \ddots & \ddots & & & & \\ & & & -1 & 2 & -1 & & \\ & & & & c & d & & \end{bmatrix}. \quad (5)$$

Values $a, b, c, d \in \mathbb{R}$ can be obtained based on *boundary conditions* (Dirichlet and Neumann) assumed for the continuous target signal x . Dirichlet condition assumes that signal x is zero at the boundary (resulting in *anti-symmetric* signal extension), while Neumann condition assumes that the derivative of x is zero at the boundary (resulting in *symmetric* signal extension). By applying Neumann condition at the left endpoint and Dirichlet / Neumann condition at the right endpoint of x at half- or full-sample locations (called *midpoint* and *meshpoint* respectively), eight DCT variants, *i.e.*, DCT-1 through DCT-8, are computed as eigenvectors of the corresponding matrices \mathbf{T} (5) in [47]. Note that by applying the Dirichlet condition at the left endpoint of signal x , eight *discrete sine transform* (DST) variants can also be similarly computed.

The key lesson from the derivation of DCT variants [47] is that *discrete frequencies are computed as eigenvectors of*

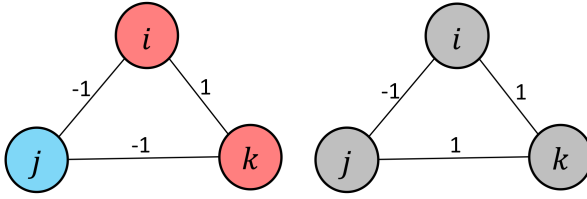


Figure 1. Two examples of three-node signed graphs ©2022 IEEE: balanced (left) and unbalanced (right).

a second difference matrix, with suitable boundary conditions applied at the boundary rows. Note that second difference matrix \mathbf{T} can be interpreted as the discrete counterpart of the *Laplace operator* ∇^2 in continuous space. Thus, $\mathbf{T}\mathbf{x} = \mathbf{0}$ is the discrete version of the *Laplace's equation* $\nabla^2 f = 0$ for continuous function f , whose twice differentiable solutions are called the *harmonic functions* [49].

E. Estimating the Precision Matrix

Given an empirical covariance matrix $\bar{\mathbf{C}}$ computed from available data, one can use the following GLASSO formulation [16], [50] to estimate a sparse inverse covariance (precision) matrix \mathbf{P} :

$$\min_{\mathbf{P}} \text{Tr}(\mathbf{P}\bar{\mathbf{C}}) - \log \det \mathbf{P} + \varphi \|\mathbf{P}\|_1 \quad (6)$$

where $\varphi > 0$ is a shrinkage parameter for the ℓ_1 -norm. (6) can be solved using a *block coordinate descent* (BCD) algorithm [16], [50]. By construction, \mathbf{P} is a *positive definite* (PD) matrix.

IV. FREQUENCIES FOR A BALANCED SIGNED GRAPH

Frequencies on graphs is a fundamental concept in GSP; we reexamine this concept here for positive graphs with self-loops, then extend it to balanced signed graphs. Specifically, we expand on two explanations in the literature to argue that eigenvectors $\{\mathbf{v}_k\}_{k=1}^N$ of a generalized graph Laplacian matrix \mathcal{L} can be defined as graph Fourier modes: i) they are successive orthonormal vectors that minimize GLR $\mathbf{x}^\top \mathcal{L} \mathbf{x}$ [17] quantifying signal variation over the graph kernel, and ii) they represent non-overlapping *nodal domains* on a graph, where the number of domains signifies total graph variation [51]. We elaborate on the graph frequency notion using GLR here; the argument using nodal domains is provided in Section 1 of the supplement.

A. Positive graphs without self-loops

Denote by $\mathbf{L} \triangleq \mathbf{D} - \mathbf{W}$ a combinatorial graph Laplacian matrix, where \mathbf{D} and \mathbf{W} are the degree and adjacency matrices, respectively, for a positive graph \mathcal{G} without self-loops. GLR $\mathbf{x}^\top \mathbf{L} \mathbf{x}$ in (1) is one measure of variation on graph \mathcal{G} for signal \mathbf{x} [17]. Specifically, we see that $\mathbf{1}^\top \mathbf{L} \mathbf{1} = 0$, and $\mathbf{x}^\top \mathbf{L} \mathbf{x} \geq 0, \forall \mathbf{x}$, since \mathbf{L} for a positive graph without self-loops is provably PSD [2]. Thus, (normalized) constant vector $(1/\sqrt{N})\mathbf{1}$ achieves the *minimal* variation. Further, it is *maximally sign-smooth* w.r.t. graph \mathcal{G} , defined as follows.

Definition 2. A signal is *maximally sign-smooth*⁵ (MS) w.r.t.

⁵While this MS definition may be obvious for a positive graph, it is useful when defining frequencies in a balanced signed graph in Section IV-C.

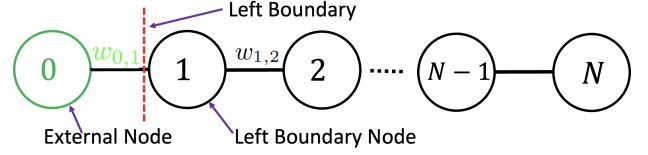


Figure 2. A line graph with N nodes, where node 1 is a left boundary node connected to external node 0 via an edge with weight $W_{0,1}$.

positive graph \mathcal{G} , if for each connected node pair $(i, j) \in \mathcal{E}$ with edge weight $W_{i,j} > 0$ describing positive correlation, $\text{sign}(x_i) = \text{sign}(x_j)$.

In other words, the lowest graph frequency $(1/\sqrt{N})\mathbf{1}$ is MS and has no zero-crossings⁶ w.r.t. positive graph \mathcal{G} . This is analogous to the constant signal (DC component) in DCT-2 for a 1D regular kernel [47]. Note that this MS notion⁷ focuses on zero-crossings and is invariant to scaling: if signal \mathbf{x} is MS, so is $c\mathbf{x}, \forall c \in \mathbb{R}$. Note also that a MS signal maps to a single nodal domain (see Section 1 of the supplement for details).

Next, each successive eigenvector \mathbf{v}_k of \mathbf{L} can be viewed as the unit-norm argument that minimizes GLR $\mathbf{x}^\top \mathbf{L} \mathbf{x}$ (which is a *Rayleigh quotient* [52]) while being orthogonal to previous eigenvectors $\mathbf{v}_i, \forall i < k$:

$$\mathbf{v}_k = \arg \min_{\mathbf{x} \perp \{\mathbf{v}_i\}_{i=1}^{k-1}, \|\mathbf{x}\|_2=1} \mathbf{x}^\top \mathbf{L} \mathbf{x}. \quad (7)$$

Further, by the definition of eigenvalues and eigenvectors,

$$\mathbf{v}_k^\top \mathbf{L} \mathbf{v}_k = \lambda_k, \quad \forall k \quad (8)$$

where $\lambda_k \geq 0$ is the eigenvalue associated with eigenvector \mathbf{v}_k , and $\lambda_{k+1} \geq \lambda_k, \forall k$. Thus, starting from MS $\mathbf{v}_1 = (1/\sqrt{N})\mathbf{1}$, eigenvectors $\{\mathbf{v}_k\}_{k=1}^N$ have increasing variation on graph \mathcal{G} , quantified by corresponding eigenvalues $\{\lambda_k\}_{k=1}^N$, as k increases. Hence, it is natural to interpret eigenvectors $\{\mathbf{v}_k\}_{k=1}^N$ as graph frequency components (Fourier modes) [40].

B. Positive graphs with self-loops

We next generalize graph \mathcal{G} to include self-loops. As discussed in Section III-A, a generalized graph Laplacian $\mathcal{L} \triangleq \mathbf{D} - \mathbf{W} + \text{diag}(\mathbf{W})$ incorporates self-loops into its definition. Motivated by DCT variants obtained from second difference matrices with different boundary conditions as discussed in Section III-D, we interpret a self-loop of a given node as a consequence of a boundary condition for that node. We dissect this interpretation for a weighted line graph next.

Consider a weighted line graph \mathcal{G} without self-loops with nodes $1, \dots, N$ as shown in Fig. 2. The corresponding tridiagonal generalized graph Laplacian \mathcal{L} is

$$\mathcal{L} = \begin{bmatrix} W_{1,2} & -W_{1,2} & 0 & \dots & 0 \\ -W_{1,2} & W_{1,2} + W_{2,3} & -W_{2,3} & \dots & 0 \\ & & \ddots & & \\ 0 & 0 & \dots & -W_{N-1,N} & W_{N-1,N} \end{bmatrix}. \quad (9)$$

⁶A signal \mathbf{x} on a positive graph has a zero-crossing at an edge $(i, j) \in \mathcal{E}$ if $W_{i,j} > 0$ and $\text{sign}(x_i)\text{sign}(x_j) = -1$.

⁷By definition 2, a MS signal \mathbf{x} is not unique and may contain high-frequency components $\mathbf{x} = \mathbf{v}_1 + \sum_{k=2}^N c_k \mathbf{v}_k$. However, since \mathbf{x} has no zero crossings, most signal energy still resides in the lowest frequency.

Given $\mathbf{x} \in \mathbb{R}^N$, the j th entry of $\mathcal{L}\mathbf{x}$, for $2 \leq j \leq N-1$, is

$$(\mathcal{L}\mathbf{x})_j = -W_{j-1,j}x_{j-1} + (W_{j-1,j} + W_{j,j+1})x_j - W_{j,j+1}x_{j+1}. \quad (10)$$

In GSP, $(\mathcal{L}\mathbf{x})_j$ is known as the *second difference* of graph signal \mathbf{x} at node j [1], [2]. Applying (10) to the left *boundary node* 1, we get

$$(\mathcal{L}\mathbf{x})_1 = -W_{0,1}x_0 + (W_{0,1} + W_{1,2})x_1 - W_{1,2}x_2, \quad (11)$$

which involves *external* node x_0 connected to graph \mathcal{G} via edge weight $W_{0,1}$, where $W_{0,1} > 0$, beyond the left boundary.

Like 1D DCT, there are two possible boundary conditions to consider: Dirichlet and Neumann [47]. For Dirichlet condition, continuous signal x is assumed zero at the *midpoint*⁸ between discrete samples x_0 and x_1 , and hence $x_0 = -x_1$ (anti-symmetric signal extension). Thus, (11) becomes

$$(\mathcal{L}\mathbf{x})_1 = (2W_{0,1} + W_{1,2})x_1 - W_{1,2}x_2. \quad (12)$$

(12) is equivalent to a linear operation on discrete \mathbf{x} using a generalized graph Laplacian \mathcal{L} with self-loop of weight $2W_{0,1}$ at node 1. Thus, we can conclude with the following lemma:

Lemma 2. *Dirichlet boundary condition on a graph kernel with an external node connected with edge weight w leads to a self-loop of weight $2w$ at the corresponding boundary node.*

Note that because weight w of the edge connected to the external node is assumed positive here, like other edge weights, self-loop weight $2w$ is also positive.

For Neumann condition, the derivative of continuous x is assumed zero at midpoint between samples x_0 and x_1 , and hence $x_0 = x_1$ (symmetric signal extension). In this case, (11) becomes $(\mathcal{L}\mathbf{x})_1 = W_{1,2}x_1 - W_{1,2}x_2$. Thus, we conclude with the following lemma:

Lemma 3. *Neumann boundary condition on a graph kernel with an external node connected with an edge does not change the Laplacian matrix of the internal graph.*

For a general graph \mathcal{G} beyond a line graph, any node can be interpreted as a boundary node. Thus, a generalized graph Laplacian \mathcal{L} with any number of positive self-loops is a valid second difference matrix with boundary conditions. By Lemma 1 in [19], there exists a strictly positive first eigenvector \mathbf{v}_1 for a generalized graph Laplacian matrix corresponding to an irreducible positive graph. \mathbf{v}_1 is MS by Definition 2, and by (7), eigenvectors $\{\mathbf{v}_k\}_{k=1}^N$ have increasing graph variations as k increases, quantified by $\{\lambda_k\}_{k=1}^N$. Thus, we consider eigenvectors $\{\mathbf{v}_k\}_{k=1}^N$ of \mathcal{L} graph frequency components for \mathcal{G} . We state the more general definition:

Definition 3. *Eigenvectors $\{\mathbf{v}_k\}_{k=1}^N$ of a PSD generalized graph Laplacian \mathcal{L}^* for a positive graph \mathcal{G}^* with self-loops are graph frequency components (Fourier modes) for \mathcal{G}^* .*

Remark: One can easily prove via GCT that generalized Laplacian \mathcal{L} for a positive graph \mathcal{G} with positive self-loops is PSD with $\lambda_1 \geq 0$ [2]. Thus, spectral shift $\mathcal{L}^* = \mathcal{L} - \alpha\lambda_1\mathbf{I}$,

⁸Applying Dirichlet and Neumann boundary conditions at *meshpoint* instead of midpoint is also possible [47], but will lead to asymmetric second difference matrices and thus is neglected here for simplicity.

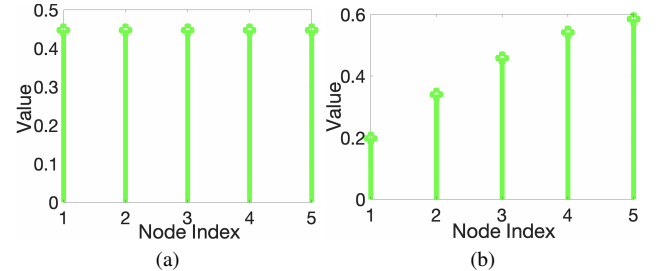


Figure 3. First eigenvector \mathbf{v}_1 of the line graph in Fig. 2 for $N = 5$ and $W_{i,j} = 1, \forall (i,j) \in \mathcal{E}$: (a) without any self-loops; (b) with a self-loop with weight 0.8 at the left boundary node 1.

for $\alpha \leq 1$, is also PSD and has the same eigenvectors (frequency components) $\{\mathbf{v}_k\}_{k=1}^N$ as \mathcal{L} . Definition 3 includes \mathcal{L} and its PSD spectral shifts \mathcal{L}^* corresponding to positive graphs \mathcal{G}^* with positive / negative self-loops. Our definition generalizes previous graph frequency definition defined using combinatorial graph Laplacians for positive graphs without self-loops [40] to positive graphs with self-loops.

Fig. 3(a) and (b) show the first eigenvectors for a line graph without self-loops and one with a single self-loop at node 1, respectively. We see that the lone positive self-loop reduces the relative magnitude of signal sample at node 1, due to the cost term $W_{1,1}x_1^2$ in the second sum of GLR (1). The practical implications of our graph frequency definition are discussed later in Section V-B.

C. Balanced Signed Graph

Consider next a balanced signed graph $\mathcal{G} = (\mathcal{V}, \mathcal{E}, \mathbf{W})$ with nodes \mathcal{V} , positive and negative inter-node edges, \mathcal{E}^+ and \mathcal{E}^- , where $\mathcal{E} = \mathcal{E}^+ \cup \mathcal{E}^-$, and adjacency matrix \mathbf{W} . \mathcal{G} may contain self-loops i , where $W_{i,i} \neq 0$. By Theorem 1, nodes set \mathcal{V} can be partitioned into blue and red subsets, \mathcal{V}_b and \mathcal{V}_r , such that

- 1) $(i, j) \in \mathcal{E}^+$ implies that either $i, j \in \mathcal{V}_b$ or $i, j \in \mathcal{V}_r$.
- 2) $(i, j) \in \mathcal{E}^-$ implies that either $i \in \mathcal{V}_b$ and $j \in \mathcal{V}_r$, or $i \in \mathcal{V}_r$ and $j \in \mathcal{V}_b$.

We generalize the MS notion defined in Definition 2 to signed graphs with the following definition.

Definition 4. *A signal is maximally sign-smooth (MS) w.r.t. signed graph \mathcal{G} , if for each connected node pair $(i, j) \in \mathcal{E}$ with edge weight $W_{i,j} > 0$ ($W_{i,j} < 0$) describing positive (negative) correlation, $\text{sign}(x_i) = \text{sign}(W_{i,j}) \text{sign}(x_j)$.*

A MS signal \mathbf{x} w.r.t. signed graph \mathcal{G} has *consistent zero-crossings*—each connected sample pair (i, j) have signs consistent with the encoded correlation $W_{i,j}$, i.e., $\text{sign}(x_i)\text{sign}(x_j) = \text{sign}(W_{i,j})$. A corollary of Theorem 1 is that there exists a MS signal \mathbf{x} for a balanced signed graph \mathcal{G} —by assigning strictly positive / negative sample values to blue / red nodes, \mathcal{V}_b and \mathcal{V}_r , respectively.

Like positive graphs, we interpret GLR $\mathbf{x}^\top \mathcal{L}\mathbf{x}$ as a measure of graph variation for signal \mathbf{x} on a balanced signed graph \mathcal{G} . To better understanding this interpretation, we first derive a positive graph \mathcal{G}' from a balanced signed graph \mathcal{G} as follows.

Without loss of generality, we first exchange rows / columns of \mathcal{L} so that blue nodes have smaller indices than red nodes. Thus, \mathcal{L} can be written as a 2×2 block matrix:

$$\mathcal{L} = \begin{bmatrix} \mathcal{L}_{11} & \mathcal{L}_{12} \\ \mathcal{L}_{12}^\top & \mathcal{L}_{22} \end{bmatrix}, \quad (13)$$

where off-diagonal terms in \mathcal{L}_{11} and \mathcal{L}_{22} are non-positive stemming from non-negative edge weights $W_{i,j} \geq 0$ connecting same-color nodes, and entries in \mathcal{L}_{12} are non-negative stemming from non-positive edge weights $W_{i,j} \leq 0$ connecting different-color nodes.

Next, we define a *similarity transform* \mathcal{L}' of \mathcal{L} :

$$\begin{aligned} \mathcal{L}' &= \begin{bmatrix} \mathbf{I}_b & \mathbf{0} \\ \mathbf{0} & -\mathbf{I}_r \end{bmatrix} \begin{bmatrix} \mathcal{L}_{11} & \mathcal{L}_{12} \\ \mathcal{L}_{12}^\top & \mathcal{L}_{22} \end{bmatrix} \begin{bmatrix} \mathbf{I}_b & \mathbf{0} \\ \mathbf{0} & -\mathbf{I}_r \end{bmatrix} \\ &= \begin{bmatrix} \mathcal{L}_{11} & -\mathcal{L}_{12} \\ -\mathcal{L}_{12}^\top & \mathcal{L}_{22} \end{bmatrix}, \end{aligned} \quad (14)$$

where \mathbf{I}_b is a $|\mathcal{V}_b| \times |\mathcal{V}_b|$ identity matrix and $|\mathcal{V}_b|$ is the number of blue nodes in \mathcal{G} . We interpret \mathcal{L}' as a generalized graph Laplacian for a positive graph \mathcal{G}' derived from \mathcal{G} , where \mathcal{G}' retains positive edges \mathcal{E}^+ , but for each negative edge in \mathcal{E}^- , \mathcal{G}' switches its sign; *i.e.*, \mathcal{G}' has weight matrix \mathbf{W}' where

$$W'_{i,j} = \begin{cases} W_{i,j} & \text{if } (i,j) \in \mathcal{E}^+ \\ -W_{i,j} & \text{if } (i,j) \in \mathcal{E}^- \end{cases}. \quad (15)$$

Moreover, as a similarity transform, \mathcal{L} and \mathcal{L}' have the same eigenvalues, and an eigenvector \mathbf{v}'_k for \mathcal{L}' maps to an eigenvector \mathbf{v}_k for \mathcal{L} , *i.e.*,

$$\mathbf{v}_k = \begin{bmatrix} \mathbf{I}_b & \mathbf{0} \\ \mathbf{0} & -\mathbf{I}_r \end{bmatrix} \mathbf{v}'_k, \quad \mathbf{v}'_k^\top \mathcal{L}' \mathbf{v}'_k = \mathbf{v}_k^\top \mathcal{L} \mathbf{v}_k = \lambda_k. \quad (16)$$

(16) implies that if \mathcal{L} is PSD, then \mathcal{L}' is also PSD.

By (16), there is a one-to-one mapping of eigenvector \mathbf{v}'_k in positive graph \mathcal{G}' to \mathbf{v}_k in balanced signed graph \mathcal{G} , with *exactly* the same graph variation quantified by eigenvalue λ_k . $\{\mathbf{v}'_k\}_{k=1}^N$ of PSD \mathcal{L}' are defined frequency components for positive graph \mathcal{G}' by Definition 3. Hence, $\{\mathbf{v}'_k\}_{k=1}^N$ must also be graph frequencies for balanced signed graph \mathcal{G} .

Definition 5. Eigenvectors $\{\mathbf{v}_k\}_{k=1}^N$ of a PSD generalized Laplacian \mathcal{L} for a balanced signed graph \mathcal{G} with self-loops are graph frequency components (Fourier modes) for \mathcal{G} .

We show that first eigenvector \mathbf{v}_1 of balanced signed graph \mathcal{G} is MS. Lemma 1 in [19] states that first eigenvector \mathbf{v}'_1 for a generalized graph Laplacian matrix \mathcal{L}' corresponding to an irreducible, positive graph \mathcal{G}' has strictly positive entries. Thus, by (16), entries in \mathbf{v}_1 are strictly positive on blue nodes and strictly negative on red nodes (or vice versa). Hence, \mathbf{v}_1 is MS on \mathcal{G} . See Fig. 4 for an illustration. Note that if signed graph \mathcal{G} is not balanced, then first eigenvector \mathbf{v}_1 for the corresponding generalized graph Laplacian \mathcal{L} would not be MS.

V. SIGNAL RECONSTRUCTION FROM SAMPLES

We formulate a MAP estimation problem to reconstruct a graph signal $\mathbf{x} \in \mathbb{R}^N$ from Gaussian-noise-corrupted samples $\mathbf{y} \in \mathbb{R}^M$, $M < N$, for a given graph \mathcal{G} (possibly with self-loops). The solution to the formulated problem leads to a graph sampling objective that we will optimize in the sequel.

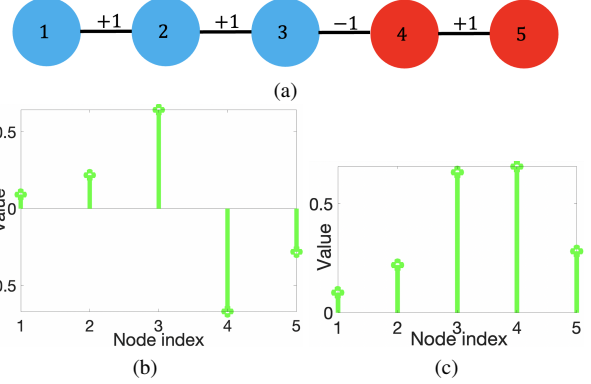


Figure 4. (a) An example of a balanced signed graph \mathcal{G} (b) the first eigenvector \mathbf{v}_1 of the balanced signed graph in (a). (c) the first eigenvector \mathbf{v}'_1 of the positive graph \mathcal{G}' derived from the balanced signed graph \mathcal{G} in (a).

A. Noise Model

First, denote by $\mathbf{H} \in \{0, 1\}^{M \times N}$ a sampling matrix that selects M samples \mathbf{y} from N original samples \mathbf{x} . \mathbf{H} can be defined as

$$H_{i,j} = \begin{cases} 1, & \text{if } i\text{th selected sample is } x_j \\ 0, & \text{otherwise.} \end{cases} \quad (17)$$

We assume that \mathbf{y} is corrupted by zero-mean, independent and identically distributed (iid) Gaussian noise of variance σ^2 . Thus, the formation model for \mathbf{y} is

$$\mathbf{y} = \mathbf{H}\mathbf{x} + \mathbf{e}, \quad (18)$$

where $\mathbf{e} \in \mathbb{R}^M$ is the additive noise. Denote by \mathbf{x} , \mathbf{e} and \mathbf{y} the realizations of random vectors \mathbf{X} , \mathbf{E} , and \mathbf{Y} , respectively, where \mathbf{X} represents the noise-free original signal, \mathbf{Y} represents the noisy sampled signal, and \mathbf{E} represents the noise.

B. MAP Formulation for Signal Reconstruction

We reconstruct signal \mathbf{x} from samples \mathbf{y} by solving a MAP formulated optimization problem. Given observed \mathbf{y} , we seek the most probable signal \mathbf{x} :

$$\mathbf{x}^* = \arg \max_{\mathbf{x}} f(\mathbf{Y} = \mathbf{y} | \mathbf{X} = \mathbf{x}) g(\mathbf{X} = \mathbf{x}), \quad (19)$$

where $f(\mathbf{Y} = \mathbf{y} | \mathbf{X} = \mathbf{x})$ is the *likelihood* of \mathbf{y} given \mathbf{x} , and $g(\mathbf{X} = \mathbf{x})$ is the *signal prior* for \mathbf{x} .

1) *Likelihood function*: Since \mathbf{e} in (18) is a zero-mean iid Gaussian noise with variance σ^2 , the probability density of \mathbf{E} is $\mathcal{N}(\mathbf{0}, \sigma^2 \mathbf{I})$. Thus, the likelihood for \mathbf{y} given \mathbf{x} is

$$f(\mathbf{Y} = \mathbf{y} | \mathbf{X} = \mathbf{x}) \propto \exp \left\{ -\frac{\|\mathbf{y} - \mathbf{H}\mathbf{x}\|_2^2}{2\sigma^2} \right\}. \quad (20)$$

2) *Signal prior*: We assume that target signal \mathbf{x} is smooth w.r.t. a defined graph \mathcal{G} (to be determined) [1], [2], [4], [5]. Specifically, we define the signal prior probability as

$$g(\mathbf{X} = \mathbf{x}) \propto \exp \left\{ -\mathbf{x}^\top \mathcal{L} \mathbf{x} \right\}, \quad (21)$$

meaning that signal \mathbf{x} with small GLR $\mathbf{x}^\top \mathcal{L} \mathbf{x}$ w.r.t. graph \mathcal{G} specified by generalized Laplacian \mathcal{L} has higher probability than a signal with large GLR. Another interpretation of (21) is that \mathbf{X} is a zero-mean *Gaussian Markov random field*

(GMRF) [53] over \mathcal{G} , *i.e.*, $\mathbf{X} \sim \mathcal{N}(\mathbf{0}, \mathcal{L}^{-1})$, where \mathcal{L}^{-1} is a covariance matrix for \mathbf{X} .

To obtain \mathcal{L} , given a training set of S graph signals $\mathcal{X} = \{\mathbf{x}_1, \dots, \mathbf{x}_S\}$, we first compute an empirical covariance matrix $\bar{\mathbf{C}}$, then employ GLASSO, as discussed in Section III-E, to compute a sparse precision matrix \mathbf{P} , which we interpret as \mathcal{L} . Note that because \mathbf{P} computed from GLASSO is in general a PD matrix with positive and negative off-diagonal terms, $\mathcal{L} = \mathbf{P}$ is a generalized Laplacian for an *unbalanced* signed graph with self-loops. We discuss our approximation to a balanced graph in Section VII.

3) *Formulation for signal reconstruction*: Combining (19), (20), and (21), we construct signal \mathbf{x}^* from samples \mathbf{y} by solving

$$\mathbf{x}^* = \arg \max_{\mathbf{x}} \exp \left\{ -\frac{\|\mathbf{y} - \mathbf{Hx}\|_2^2}{2\sigma^2} - \mathbf{x}^\top \mathcal{L} \mathbf{x} \right\}. \quad (22)$$

We rewrite the objective by minimizing the negative logarithm of (22) instead, resulting in

$$\mathbf{x}^* = \arg \min_{\mathbf{x}} \|\mathbf{Hx} - \mathbf{y}\|_2^2 + \mu \mathbf{x}^\top \mathcal{L} \mathbf{x}, \quad (23)$$

where $\mu = 2\sigma^2 > 0$ is a weight parameter trading off the fidelity $\|\mathbf{Hx} - \mathbf{y}\|_2^2$ with the prior $\mathbf{x}^\top \mathcal{L} \mathbf{x}$. Since terms in (23) are convex and quadratic, the solution \mathbf{x}^* to (23) is computed by solving the following linear system:

$$\underbrace{(\mathbf{H}^\top \mathbf{H} + \mu \mathcal{L})}_{\mathbf{B}} \mathbf{x}^* = \mathbf{H}^\top \mathbf{y}. \quad (24)$$

Specifically, (24) is a system of linear equations with a unique solution \mathbf{x}^* if \mathbf{B} is PD. Given \mathcal{L} computed from GLASSO is PD, \mathbf{B} is also PD by Weyl's inequality [54].

Remark: Our notion of graph frequencies has practical implications. A MAP formulation with GLR as signal prior (21)—where \mathcal{L} is a generalized Laplacian for a balanced signed graph—means favoring low-pass signals with small graph variations by Definition 5. This means that an optimal solution to a MAP formulation regularized with GLR is *always* a LP filter. This improves the interpretability of the derived filtering system; we know that the system is biased towards signals with minimum inconsistent zero-crossings, with MS \mathbf{v}_1 having no inconsistent zero-crossings at all. In contrast, if \mathcal{L} is a Laplacian to an unbalanced signed graph, then we would not know if the system promotes a MS signal.

VI. SIGNED GRAPH SAMPLING

A. Objective Definition

Our sampling objective is to minimize the condition number of \mathbf{B} —ratio of largest to smallest eigenvalues $\rho = \lambda_{\max}(\mathbf{B})/\lambda_{\min}(\mathbf{B})$ —via selection of \mathbf{H} to optimize the stability of the linear system (24). Since $\lambda_{\max}(\mathbf{B})$ can be upper-bounded [10], we maximize $\lambda_{\min}(\mathbf{B})$ instead:

$$\max_{\mathbf{H} \mid \text{Tr}(\mathbf{H}^\top \mathbf{H}) \leq M} \lambda_{\min}(\mathbf{B}), \quad (25)$$

where $\text{Tr}(\cdot)$ is the trace of a matrix. Maximizing $\lambda_{\min}(\mathbf{B})$ —called *E-optimality* in optimal design [32]—is equivalent to minimizing the worst-case signal reconstruction error between a solution of (24) and the ground-truth signal [10].

B. GDA Sampling for Positive Graphs

Given generalized graph Laplacian $\mathcal{L} = \mathbf{P}$ computed from GLASSO, optimization (25) is equivalent to sampling on a signed graph with self-loops. To the best of our knowledge, sampling on signed graphs has not been studied in the graph sampling literature [7], [10], [24], [30], [55].

We first overview previous GDAS sampling [10] for positive graph without self-loops, from which we will generalize later. Assuming \mathcal{L} is a combinatorial graph Laplacian matrix $\mathcal{L} = \mathbf{D} - \mathbf{W}$ for a positive graph \mathcal{G} without self-loops, all Gershgorin disc left-ends of \mathcal{L} are at 0 exactly, *i.e.*, $c_i - r_i = D_{i,i} - \sum_{j \neq i} |W_{i,j}| = 0, \forall i$. Under this condition, GDAS can be employed to approximately solve (25) with roughly linear-time complexity.

In a nutshell, GDAS maximizes *smallest eigenvalue lower bound* $\lambda_{\min}^-(\mathbf{C})$ of a similar-transformed matrix $\mathbf{C} = \mathbf{S}\mathbf{B}\mathbf{S}^{-1}$ of \mathbf{B} , *i.e.*, $\lambda_{\min}^-(\mathbf{C}) \leq \lambda_{\min}(\mathbf{C}) = \lambda_{\min}(\mathbf{B})$. $\mathbf{S} = \text{diag}(s_1, \dots, s_N)$ is a diagonal matrix with scalars $s_i > 0$ on its diagonal. By GCT [56], $\lambda_{\min}^-(\mathbf{C}) = \min_i(c_i - r_i)$ is the smallest Gershgorin disc left-end of matrix \mathbf{C} . Given a target threshold $T > 0$, GDAS (roughly) realigns all disc left-ends of \mathbf{C} to T via two operations, expending as few samples K as possible in the process.

The two basic disc operations for a given target T are:

- 1) *Disc Shifting*: sample a node i in the graph means that the (i, i) -th entry of $\mathbf{H}^\top \mathbf{H}$ in \mathbf{B} becomes 1 and shifts disc center of row i of \mathbf{C} to the right by 1.
- 2) *Disc Scaling*: select scalar $s_i > 1$ to increase disc radius of row i corresponding to sampled node i , thus decreasing disc radii of neighboring nodes j due to s_i^{-1} in \mathbf{S}^{-1} , and moving disc left-ends of rows j to the right.

We demonstrate these two disc operations in GDAS using an example from [57]. Consider a 4-node line graph, shown in Fig. 5. Suppose we first sample node 3. If $\mu = 1$, then the coefficient matrix \mathbf{B} is as shown in Fig. 6a, after $(3, 3)$ entry is updated. Correspondingly, Gershgorin disc ψ_3 's left-end of row 3 moves from 0 to 1, as shown in Fig. 6d (red dots and blue arrows represent disc centers and radii, respectively).

Next, we scale disc ψ_3 of sampled node 3: apply scalar $s_3 > 1$ to row 3 of \mathbf{B} to move disc ψ_3 's left-end left to threshold T exactly, as shown in Fig. 6b. Concurrently, scalar $1/s_3$ is applied to the third column, and thus the disc radii of ψ_2 and ψ_4 are reduced due to scaling of $w_{2,3}$ and $w_{4,3}$ by $1/s_3$. Note that diagonal entry $(3, 3)$ of \mathbf{B} (*i.e.*, ψ_3 's disc center) is unchanged, since the effect of s_3 is offset by $1/s_3$. We observe that by expanding disc ψ_3 's radius, the disc left-ends of its neighbors (*i.e.*, ψ_2 and ψ_4) move right beyond bound T as shown in Fig. 6e.

Subsequently, scalar $s_2 > 1$ for disc ψ_2 is applied to expand its radius, so that ψ_2 's left-end moves to T . Again, this has the effect of shrinking the disc radius of neighboring node 1, pulling its left-end right beyond T , as shown in Fig. 6c and Fig. 6f. At this point, left-ends of all discs have moved beyond T , and thus we conclude that by sampling a single node 3, smallest eigenvalue λ_{\min} of \mathbf{B} is lower-bounded by T .

In practice, an appropriate threshold T for given sampling budget M can be identified via binary search, since T and the

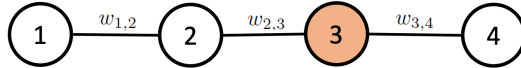


Figure 5. An illustrative example of a 4-node line graph from [57].

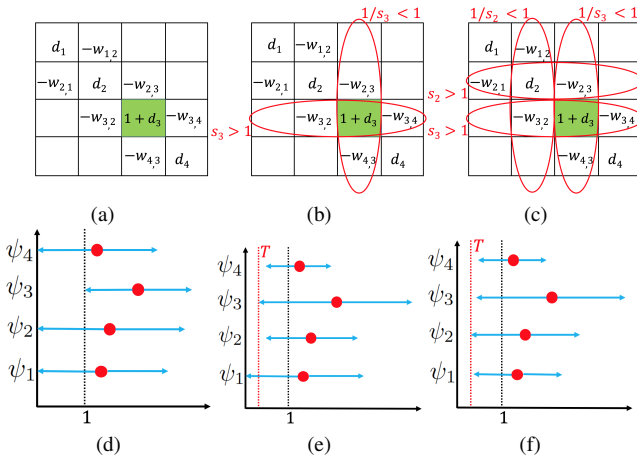


Figure 6. An illustration of GDAS from [57] ©2019 IEEE. (a) sampling node 3. (b) scaling node 3. (c) scaling nodes 2 and 3. (d) Discs after sampling node 3. (e) Discs after scaling node 3. (f) Discs after scaling nodes 2 and 3.

required number samples K to move all disc left-ends beyond T are proportional. See [57] for further details.

C. GDA Sampling for Signed Graphs

In the previous discussion of GDAS for positive graphs without self-loops, disc left-ends are initially aligned at the same value 0, then via a sequence of disc shifting and scaling operations, become (roughly) aligned at threshold T . However, \mathcal{L} computed from GLASSO is a generalized graph Laplacian corresponding to an irreducible⁹ signed graph \mathcal{G} with self-loops. This means that the Gershgorin disc left-ends of \mathcal{L} are not initially aligned at the same exact value, and GDAS sampling cannot be used directly.

Fortunately, a recent linear algebraic theorem GDPA [19] provides the mathematical machinery to align disc left-ends. Specifically, GDPA proves that Gershgorin disc left-ends of a generalized graph Laplacian matrix \mathcal{L}_B for an irreducible, *balanced*, signed graph \mathcal{G}_B can be aligned *exactly* at $\lambda_{\min}(\mathcal{L}_B)$ via similarity transform $\mathbf{S}\mathcal{L}_B\mathbf{S}^{-1}$, where $\mathbf{S} = \text{diag}(v_1^{-1}, \dots, v_N^{-1})$, and $\mathbf{v} = [v_1 \dots v_N]^\top$ is the first eigenvector of \mathcal{L}_B corresponding to $\lambda_{\min}(\mathcal{L}_B)$. First eigenvector \mathbf{v} of \mathcal{L}_B can be computed efficiently using *Locally Optimal Block Preconditioned Conjugate Gradient* (LOBPCG) [59] in linear time, given \mathcal{L}_B is sparse.

Leveraging GDPA, we employ the following recipe to solve the sampling problem (25) for \mathcal{L} approximately.

Step 1: Approximate $\mathcal{G} = (\mathcal{V}, \mathcal{E}, \mathbf{W})$ with a balanced graph $\mathcal{G}_B = (\mathcal{V}, \mathcal{E}_B, \mathbf{W}_B)$ while satisfying the following condition:

$$\lambda_{\min}(\mathbf{H}^\top \mathbf{H} + \mu \mathcal{L}_B) \leq \lambda_{\min}(\mathbf{H}^\top \mathbf{H} + \mu \mathcal{L}). \quad (26)$$

Step 2: Given \mathcal{L}_B , perform similarity transform

⁹An irreducible graph \mathcal{G} means that there exists a path from any node in \mathcal{G} to any other node in \mathcal{G} [58].

$\mathcal{L}_p = \mathbf{S}\mathcal{L}_B\mathbf{S}^{-1}$, so that disc left-ends of matrix \mathcal{L}_p are aligned exactly at $\lambda_{\min}(\mathcal{L}_p) = \lambda_{\min}(\mathcal{L}_B)$.

Step 3: Employ GDAS sampling method [10] on \mathcal{L}_p to maximize $\lambda_{\min}^-(\mathbf{H}^\top \mathbf{H} + \mu \mathcal{L}_p)$.

Clearly, one should obtain a balanced graph \mathcal{G}_B that induces a *tight* lower bound $\lambda_{\min}(\mathbf{H}^\top \mathbf{H} + \mu \mathcal{L}_B)$ for $\lambda_{\min}(\mathbf{H}^\top \mathbf{H} + \mu \mathcal{L})$ in (26). Thus, we next define an optimization objective for graph balancing and propose a fast balancing algorithm.

D. Graph Balancing Formulation

We first show that if we obtain a balanced graph \mathcal{G}_B such that $\mathbf{L} - \mathbf{L}_B$ is a PSD matrix (*i.e.*, $\mathbf{L} - \mathbf{L}_B \succeq 0$), then (26) will be satisfied, where \mathbf{L} and \mathbf{L}_B are combinatorial graph Laplacian matrices for graphs \mathcal{G} and \mathcal{G}_B , respectively.

Theorem 4. *Given two undirected graphs $\mathcal{G} = (\mathcal{V}, \mathcal{E}, \mathbf{W})$ and $\mathcal{G}_B = (\mathcal{V}, \mathcal{E}_B, \mathbf{W}_B)$ with the same set of self-loops, if $\mathbf{L} - \mathbf{L}_B \succeq 0$, then (26) is satisfied.*

Proof. Since $\mathbf{L} - \mathbf{L}_B \succeq 0$, we can write

$$\mathbf{x}^\top \mathbf{L} \mathbf{x} \geq \mathbf{x}^\top \mathbf{L}_B \mathbf{x}, \quad \forall \mathbf{x} \in \mathbb{R}^N. \quad (27)$$

Moreover, since the two graphs have the same set of self-loops, $\text{diag}(\mathbf{W}) = \text{diag}(\mathbf{W}_B)$, where \mathbf{W} and \mathbf{W}_B are adjacency matrices of graphs \mathcal{G} and \mathcal{G}_B respectively. Then, due to (27), we can write that, $\forall \mathbf{x} \in \mathbb{R}^N$,

$$\underbrace{\mathbf{x}^\top (\mathbf{L} + \text{diag}(\mathbf{W})) \mathbf{x}}_{\mathcal{L}} \geq \underbrace{\mathbf{x}^\top (\mathbf{L}_B + \text{diag}(\mathbf{W}_B)) \mathbf{x}}_{\mathcal{L}_B}. \quad (28)$$

Consequently,

$$\mathbf{x}^\top (\mathbf{H}^\top \mathbf{H} + \mu \mathcal{L}) \mathbf{x} \geq \mathbf{x}^\top (\mathbf{H}^\top \mathbf{H} + \mu \mathcal{L}_B) \mathbf{x}. \quad (29)$$

Denote by \mathbf{u} the unit-norm eigenvector corresponding to the smallest eigenvalue of $\mathbf{H}^\top \mathbf{H} + \mu \mathcal{L}$. Hence,

$$\lambda_{\min}(\mathbf{H}^\top \mathbf{H} + \mu \mathcal{L}) = \mathbf{u}^\top (\mathbf{H}^\top \mathbf{H} + \mu \mathcal{L}) \mathbf{u}. \quad (30)$$

By the *Min-max Theorem* [60], we can write

$$\lambda_{\min}(\mathbf{H}^\top \mathbf{H} + \mu \mathcal{L}_B) = \min_{\mathbf{x}, \|\mathbf{x}\|_2=1} \mathbf{x}^\top (\mathbf{H}^\top \mathbf{H} + \mu \mathcal{L}_B) \mathbf{x}. \quad (31)$$

By substituting $\mathbf{x} = \mathbf{u}$ in (29) and using (30) and (31), we can write

$$\begin{aligned} \lambda_{\min}(\mathbf{H}^\top \mathbf{H} + \mu \mathcal{L}) &\geq \mathbf{u}^\top (\mathbf{H}^\top \mathbf{H} + \mu \mathcal{L}_B) \mathbf{u} \\ &\geq \min_{\mathbf{x}, \|\mathbf{x}\|_2=1} \mathbf{x}^\top (\mathbf{H}^\top \mathbf{H} + \mu \mathcal{L}_B) \mathbf{x} \\ &= \lambda_{\min}(\mathbf{H}^\top \mathbf{H} + \mu \mathcal{L}_B) \end{aligned} \quad (32)$$

which concludes the proof. \square

From the proof, one can see that $\lambda_{\min}(\mathbf{H}^\top \mathbf{H} + \mu \mathcal{L}_B)$ forms a tight lower bound for $\lambda_{\min}(\mathbf{H}^\top \mathbf{H} + \mu \mathcal{L})$ when $\mathbf{x}^\top \mathbf{L}_B \mathbf{x}$ is a tight lower bound for $\mathbf{x}^\top \mathbf{L} \mathbf{x}$, $\forall \mathbf{x} \in \mathbb{R}^N$. Hence, we define our objective for a balanced graph \mathcal{G}_B to maximize $\mathbf{x}^\top \mathbf{L}_B \mathbf{x}$ subject to $\mathbf{L} - \mathbf{L}_B \succeq 0$.

Specifically, in Section V-B we assume \mathbf{x} is a realization of random vector \mathbf{X} that is a zero-mean GMRF [53] over \mathcal{G} , *i.e.*, $\mathbf{X} \sim \mathcal{N}(\mathbf{0}, \mathbf{C})$, where \mathbf{C} is the covariance matrix and

$\mathcal{L} = \mathbf{C}^{-1}$. Next, we choose a balanced graph \mathcal{G}_B to maximize the expectation of $\mathbf{X}^\top \mathbf{L}_B \mathbf{X}$ subject to $\mathbf{L} - \mathbf{L}_B \succeq 0$:

$$\begin{aligned} \mathbb{E}[\mathbf{X}^\top \mathbf{L}_B \mathbf{X}] &= \mathbb{E}[\text{Tr}(\mathbf{X}^\top \mathbf{L}_B \mathbf{X})] = \mathbb{E}[\text{Tr}(\mathbf{L}_B \mathbf{X} \mathbf{X}^\top)] \\ &= \text{Tr}(\mathbf{L}_B \mathbb{E}[\mathbf{X} \mathbf{X}^\top]) = \text{Tr}(\mathbf{L}_B \mathbf{C}). \end{aligned} \quad (33)$$

Maximizing (33) will thus promote tightness of bound (26) given $\mathbf{x} \sim \mathcal{N}(\mathbf{0}, \mathbf{C})$. We now formalize our optimization objective for graph balancing as follows:

$$\max_{\mathbf{L}_B} \text{Tr}(\mathbf{L}_B \mathbf{C}) ; \text{ s.t. } \begin{cases} \mathbf{L} - \mathbf{L}_B \succeq 0, \\ \mathbf{L}_B \in \mathcal{B} \subset \mathbb{R}^{N \times N} \end{cases} \quad (34)$$

where \mathcal{B} is the set of $N \times N$ combinatorial graph Laplacian matrices corresponding to balanced signed graphs.

Like previous graph approximation problems such as [61] where the “closest” bipartite graph is sought to approximate a given non-bipartite graph, the balanced graph approximation problem in (34) is difficult due to its combinatorial nature. Thus, similar to [61], we propose a greedy algorithm to add one “most beneficial” node at a time (with *consistent* edges) to construct a balanced graph as solution to (34).

VII. GRAPH BALANCING ALGORITHM

A. Notations and Definitions

To facilitate understanding, we first introduce the following notations and definitions.

1. We define the notion of *consistent* edges in a balanced graph, stemming from Theorem 1, as follows.

Definition 6. A *consistent edge* is a positive edge connecting two nodes of the same color, or a negative edge connecting two nodes of opposite colors. An edge that is not consistent is an *inconsistent edge*.

Using this definition, for an edge $(i, j) \in \mathcal{E}_B$, we can write

$$\beta_i \beta_j \text{sign}(W_{i,j}) = \begin{cases} 1; & \text{if } (i, j) \text{ is consistent} \\ -1; & \text{if } (i, j) \text{ is inconsistent,} \end{cases} \quad (35)$$

where β_i denotes the color assignment of node i (i.e., $\beta_i = 1$ if node i is blue and $\beta_i = -1$ if node i is red).

2. Given graph $\mathcal{G} = (\mathcal{V}, \mathcal{E}, \mathbf{W})$, we define a *bi-colored* node set $\mathcal{S} \subseteq \mathcal{V}$, where all edges connecting nodes in \mathcal{S} are consistent. Further, denote by $\mathcal{C} \subseteq \mathcal{V} \setminus \mathcal{S}$ the set of nodes in \mathcal{V} exactly one hop away from \mathcal{S} . An example of graph \mathcal{G} with sets \mathcal{C} and \mathcal{S} is shown in Fig. 7, where $\mathcal{S} = \{1, 2, 3, 4\}$ and $\mathcal{C} = \{5, 6\}$. If all nodes of graph \mathcal{G} are in set \mathcal{S} , i.e., $\mathcal{S} = \mathcal{V}$ and $\mathcal{C} = \emptyset$, then \mathcal{G} is balanced by Theorem 1.

3. Using (35), for each node $j \in \mathcal{C}$ we partition edges connecting j to \mathcal{S} into two disjoint sets: i) the set \mathcal{F}_j of consistent edges from j to \mathcal{S} when $\beta_j = 1$, and ii) the set \mathcal{H}_j of consistent edges from j to \mathcal{S} when $\beta_j = -1$. Note that \mathcal{F}_j (\mathcal{H}_j) is also the set of inconsistent edges when $\beta_j = -1$ ($\beta_j = 1$). As an illustration, an example of edge sets \mathcal{F}_j and \mathcal{H}_j connecting $j \in \mathcal{C}$ to \mathcal{S} is shown in Fig. 8, where consistent and inconsistent edges are drawn in different colors for a given value β_j . We see that if we remove inconsistent edges from $j \in \mathcal{C}$ to \mathcal{S} for a given β_j value, node j can be added to \mathcal{S} .

Algorithm 1 Solving (36)

```

1: Set  $i = 1$  and  $\beta_i = 1$ .
2: for  $j = \{1, 2, \dots, |\mathcal{C}|\}$  do
3:   for  $\beta_j = \{1, -1\}$  do
4:     if  $(f_i(\beta_i) - f_j(\beta_j)) < 0$  then
5:       Update  $i = j$  and  $\beta_i = \beta_j$ .
6:     end if
7:   end for
8: end for
9: Set  $j^* = i$  and  $\beta_{j^*} = \beta_i$ .

```

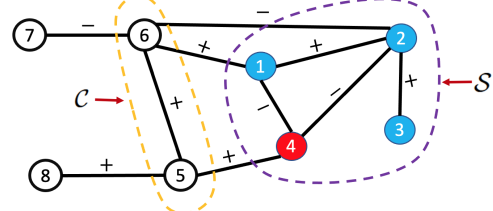


Figure 7. An example of an 8-node graph \mathcal{G} with sets $\mathcal{S} = \{1, 2, 3, 4\}$ and $\mathcal{C} = \{5, 6\}$.

4. Denote by $f_j(\beta_j)$ the value of the objective in (34) when node j is assigned color β_j and the corresponding inconsistent edges from $j \in \mathcal{C}$ to \mathcal{S} are removed. This means removing \mathcal{H}_j if $\beta_j = 1$, and removing \mathcal{F}_j if $\beta_j = -1$.

B. Greedy Balancing Algorithm

Using the above definitions, we present our iterative greedy algorithm to approximately solve (34). In a nutshell, given an unbalanced graph \mathcal{G} , we construct a corresponding balanced graph \mathcal{G}_B by adding one node at a time to set \mathcal{S} . At each iteration, we select a “most beneficial” node $j \in \mathcal{C}$ with color β_j to add to \mathcal{S} , so that the objective in (34) is locally maximized.

Specifically, first, we initialize bi-colored set \mathcal{S} with a random node i and color it blue, i.e., $\beta_i = 1$. Then, at each iteration, we select a node $j \in \mathcal{C}$ and corresponding color β_j that maximizes objective $f_j(\beta_j)$, i.e.,

$$(j^*, \beta_{j^*}^*) = \arg \max_{j \in \mathcal{C}, \beta_j \in \{-1, 1\}} f_j(\beta_j). \quad (36)$$

For given $f_j(\beta_j)$ values, solving (36) is shown in Algorithm 1 with a linear time complexity $\mathcal{O}(|\mathcal{C}|)$, where $|\mathcal{C}|$ is the number of nodes in set \mathcal{C} . We add node j^* of solution $(j^*, \beta_{j^*}^*)$ in (36) to set \mathcal{S} , assign it color $\beta_{j^*}^*$, and remove inconsistent edges from j^* to \mathcal{S} to conclude the iteration. Main steps of the algorithm are summarized as follows:

- Step 1:** Initialize set \mathcal{S} with a random node i and set $\beta_i = 1$.
- Step 2:** Compute $f_j(1)$ and $f_j(-1)$ for each $j \in \mathcal{C}$.
- Step 3:** Compute locally optimal solution $(j^*, \beta_{j^*}^*)$ for (36).
- Step 4:** Remove all inconsistent edges from $j^* \in \mathcal{C}$ to \mathcal{S} .
- Step 5:** $\mathcal{S} \leftarrow \mathcal{S} \cup j^*$.
- Step 6:** Update \mathcal{C} according to modified \mathcal{S} .
- Step 7:** Repeat steps 2-6 until $\mathcal{C} = \emptyset$.

Note that when removing inconsistent edges in step 2 (to compute $f_j(1)$ and $f_j(-1)$) and step 4, the constraint $\mathbf{L} - \mathbf{L}_B \succeq 0$ in optimization (34) must be preserved.

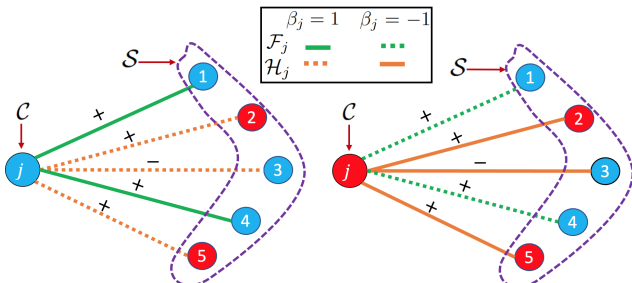


Figure 8. An example of consistent edges \mathcal{F}_j and inconsistent edges \mathcal{H}_j connecting node $j \in \mathcal{C}$ to \mathcal{S} when $\beta_j = 1$ (left), and consistent edges \mathcal{H}_j and inconsistent edges \mathcal{F}_j when $\beta_j = -1$ (right). For simplicity, we omit edges connecting nodes within set \mathcal{S} .

C. Inconsistent Positive Edge Removal

We first show that when removing a positive edge, the constraint $\mathbf{L} - \mathbf{L}_B \succeq 0$ is always maintained as formally stated in Theorem 5.

Theorem 5. *Given an undirected graph $\mathcal{G} = (\mathcal{V}, \mathcal{E}, \mathbf{W})$, removing a positive edge $(q, r) \in \mathcal{E}$ from \mathcal{G} —resulting in graph $\mathcal{G}_B = (\mathcal{V}, \mathcal{E} \setminus (q, r), \mathbf{W}_B)$ —entails $\mathbf{L} - \mathbf{L}_B \succeq 0$.*

Proof. By (1), for graph \mathcal{G} , we can write following expressions $\forall \mathbf{x} \in \mathbb{R}^N$,

$$\begin{aligned} \mathbf{x}^\top \mathbf{L} \mathbf{x} &= \sum_{(i,j) \in \mathcal{E}} W_{i,j} (x_i - x_j)^2, \\ &= W_{q,r} (x_q - x_r)^2 + \sum_{(i,j) \in \mathcal{E} \setminus (q,r)} W_{i,j} (x_i - x_j)^2. \end{aligned} \quad (37)$$

Since $W_{q,r} > 0$, we can write following inequality using (37),

$$\mathbf{x}^\top \mathbf{L} \mathbf{x} \geq \sum_{(i,j) \in \mathcal{E} \setminus (q,r)} W_{i,j} (x_i - x_j)^2 = \mathbf{x}^\top \mathbf{L}_B \mathbf{x}. \quad (38)$$

Hence, $\mathbf{L} - \mathbf{L}_B \succeq 0$, which concludes the proof. \square

Given the ease of removing inconsistent positive edges, we first remove them all before inconsistent negative edges.

D. Inconsistent Negative Edge Removal

There are two cases of removing inconsistent negative edges as discussed below.

1) *Case 1:* In this case, a negative edge can be removed while satisfying $\mathbf{L} - \mathbf{L}_B \succeq 0$ by the following theorem.

Theorem 6. *Given graph $\mathcal{G} = (\mathcal{V}, \mathcal{E}, \mathbf{W})$, a negative edge $(j, i) \in \mathcal{E}$ can be removed while maintaining $\mathbf{L} - \mathbf{L}_B \succeq 0$ if there are two previously removed positive edges $(k, j), (k, i) \in \mathcal{E}$ connected to a third node k , such that*

$$W_{p,q} \geq -2W_{j,i} \quad \text{for } (p, q) \in \{(k, j), (k, i)\}. \quad (39)$$

Proof of Theorem 6 is given in Section 2 in the supplement.

To use Theorem 6 during the algorithm iterations, we maintain a Laplacian $\mathbf{L}^d = \mathbf{L} - \mathbf{L}_B$ for graph \mathcal{G}^d that contains all augmented edges to date. When considering removal of negative edge (j, i) , we check if previously removed edges $(k, j), (k, i)$ for third node $k \in \mathcal{N}_j \cup \mathcal{N}_i$ exist in \mathcal{G}^d satisfying (39). If so, we remove edge (j, i) and add it to \mathcal{G}^d . We also

mark edges $(k, j), (k, i)$ in \mathcal{G}^d , so they will not be used for more negative edge removals in later iterations.

Denote by \mathcal{P} the set of candidates for $k \in \mathcal{N}_j \cup \mathcal{N}_i$. One approach is to choose k within candidate solution set \mathcal{P} so that $f_j^k(\beta_j)$ (i.e., value of $f_j(\beta_j)$ for a given $k \in \mathcal{P}$) is maximized, i.e.,

$$k^* = \arg \max_{k \in \mathcal{N}_j \cup \mathcal{N}_i \mid k \in \mathcal{P}} f_j^k(\beta_j). \quad (40)$$

The complexity of this check for edges $(k, j), (k, i)$ in \mathcal{G}^d is linear in the number of neighbors to nodes j and i , $|\mathcal{N}_j \cup \mathcal{N}_i|$. Assuming initial \mathcal{G} is a sparse graph, this is $\mathcal{O}(1)$.

2) *Case 2:* If an inconsistent negative edge (j, i) cannot be removed via Theorem 6 (i.e., if $|\mathcal{P}| = 0$), we update weights of two additional edges that together with (j, i) form a triangle, in order to ensure constraint $\mathbf{L} - \mathbf{L}_B \succeq 0$ is satisfied, while keeping updated edges consistent. We state this formally in Theorem 7.

Theorem 7. *Given graph $\mathcal{G} = (\mathcal{V}, \mathcal{E}, \mathbf{W})$, denote by $(j, i) \in \mathcal{E}$ an inconsistent negative edge connecting nodes $j \in \mathcal{C}$ and $i \in \mathcal{S}$ of the same color. Let $k \in \mathcal{S}$ be a node of opposite color to nodes j and i . If edge (j, i) is removed, and weights for edges (k, j) and (k, i) are updated as*

$$\tilde{W}_{p,q} = W_{p,q} + 2W_{j,i} \quad \text{for } (p, q) \in \{(k, j), (k, i)\} \quad (41)$$

then a) $\mathbf{L} - \mathbf{L}_B \succeq 0$; and b) (k, j) and (k, i) are consistent edges.

Proof of Theorem 7 is given in Section 2 in the supplement.

Fig. 9 shows how an inconsistent negative edge is removed in this case. When removing an inconsistent negative edge (j, i) from Fig. 9(left), we select node $k \in \mathcal{S}$, where $i, k \in \mathcal{S}$ are of opposite colors. If negative edges (k, i) and/or (k, j) do not exist, we create edges with zero weight $W_{k,i} = 0$ and/or $W_{k,j} = 0$, resulting in a triangle (i, k, j) .

Then, using Theorem 7, we remove edge (j, i) and update edge weights $W_{i,k}$ and $W_{k,j}$ as shown in Fig. 9(right). We see that the updated edges (k, i) and (k, j) maintain the same signs and are consistent. Further, by Theorem 7, this edge weight update ensures that $\mathbf{L} - \mathbf{L}_B \succeq 0$ remains satisfied.

Denote by \mathcal{K} the set of candidates for $k \in \mathcal{S}$. Similar to Section VII-D1, one approach is to choose k within candidate solution set \mathcal{K} so that $f_j^k(\beta_j)$ is maximized, i.e.,

$$k^* = \arg \max_{k \in \mathcal{K}} f_j^k(\beta_j). \quad (42)$$

Such an exhaustive search for each $k \in \mathcal{K}$ for large $|\mathcal{K}|$ has a high computation cost. Instead, if $|\mathcal{K}| > 1$, we select a $k \in \mathcal{K}$ within the 1-hop neighborhoods of nodes j and i :

$$k^* = \arg \max_{k \in \mathcal{N}_j \cup \mathcal{N}_i \mid k \in \mathcal{K}} f_j^k(\beta_j), \quad (43)$$

Experimental results show that there is no significant performance difference between the exhaustive approach in (42) and the approach with a reduced search space in (43).

For a given value of β_j , if $|\mathcal{K}| = 0$, then it means that there are no nodes in \mathcal{S} of opposite color to i , or more simply, all nodes in \mathcal{S} are of the same color. In this case, it suffices to

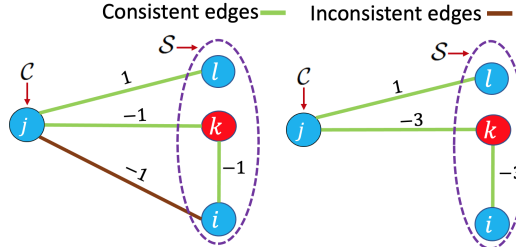


Figure 9. An example for edge weight updating. A cycle $i \rightarrow j \rightarrow k \rightarrow i$ with inconsistent negative edge (j, i) need to be removed (left); updated edge weights after removing the negative inconsistent edge (right).

color $j \in \mathcal{C}$ to be the opposite color to nodes in \mathcal{S} and remove all inconsistent positive edges to \mathcal{S} as stated in Theorem 8.

Theorem 8. *Let $j \in \mathcal{C}$ and all nodes in \mathcal{S} be of the same color. If node $j \in \mathcal{C}$ is colored to be the opposite color to nodes in \mathcal{S} and all positive edges from $j \in \mathcal{C}$ to \mathcal{S} are removed, then all remaining edges from $j \in \mathcal{C}$ to \mathcal{S} are consistent.*

Proof. When all nodes in \mathcal{S} are in the opposite color to the node $j \in \mathcal{C}$, according to Theorem 1, all negative edges from $j \in \mathcal{C}$ to \mathcal{S} are consistent while all positive edges are inconsistent. Therefore, since we remove all inconsistent positive edges, all remaining negative edges from $j \in \mathcal{C}$ to \mathcal{S} are consistent. \square

VIII. EXPERIMENTS

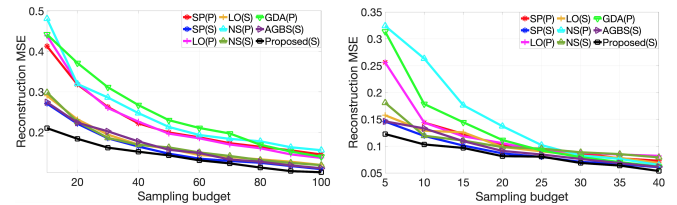
A. Experimental Setup

We present comprehensive experiments to verify the effectiveness of our proposed signed graph sampling algorithm. We used four different datasets for our experiments.

1) *Canadian Parliament Voting Records Dataset*: The first dataset consists of Canadian Parliament voting records from the 38th parliament to the 43rd parliament (2005–2021)¹⁰. This dataset contains voting records of 340 constituencies voted in 3154 elections. The votes were recorded as -1 for “no” and 1 for “yes” and 0 for “abstain / absent”. Thus, we define a signal for a given vote as $\mathbf{x} \in \{1, 0, -1\}^{340}$.

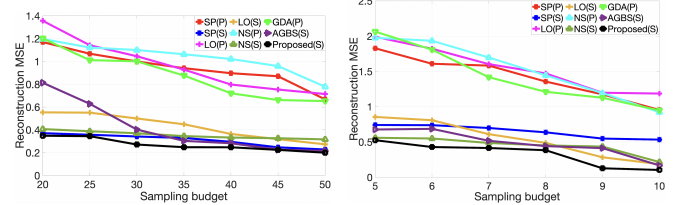
2) *US Senate Voting Records Dataset*: The second dataset consists of US Senate voting records from the 115th and 116th congress (2017–2020)¹¹. This dataset contains voting records of 100 senators in 1320 elections. Both the Canadian and US voting datasets have strong inherent anti-correlations, because voting records in the parliament / senate often show opposing positions between the two main political parties.

3) *Canadian Car Model Sales Dataset*: This dataset¹² contains Canada vehicle model monthly sales for 2019–2022. We selected 100 car models for this experiments. Each car model was a graph node, and the corresponding monthly sale was the sample value for that node. We observed that as the sales of some car models increased, the sales of some other models decreased. Hence, the sales data have anti-correlations.



(a) Canadian parliament voting dataset

(b) US senate voting dataset



(c) Canada car models sales dataset (d) Appliances ON/OFF status dataset

Figure 10. Reconstruction MSE for different sampling algorithms under different sampling budgets using GLR-reconstruction. “P” and “S” within each bracket represent the positive graph and signed graph, respectively.

4) *Almanac of Minutely Power Dataset Version 2 (AMPds2)*: AMPds2 [62] contains two years of ON/OFF status data sampled at 1-minute intervals for 15 residential appliances in a Canadian household. In our experiment, we used ON/OFF status at 104000 time instances. We defined ON / OFF status as $1 / -1$, respectively. Thus, a signal for a given time instant is defined as $\mathbf{x} \in \{1, -1\}^{15}$. Some appliance pairs have inherent anti-correlations. For example, if lights in the living room are ON, then lights in the bedrooms are often OFF.

To compute an empirical covariance matrix $\bar{\mathbf{C}}$ for each dataset, we randomly selected 90% of signals from each dataset. Then, following GLASSO formulation in Section III-E, we estimated a sparse inverse covariance matrix for each dataset, which is interpreted as a generalized graph Laplacian matrix \mathcal{L} corresponding to a signed graph. Finally, the remaining 10% of signals were used to test different graph sampling algorithms.

For competing sampling schemes that require positive graphs, we constructed a positive graph for each dataset using the following graph learning formulation in [63]:

$$\min_{\mathbf{L}} \text{Tr}(\mathbf{LK}) - \log |\mathbf{L}| \text{ subject to } \mathbf{L} \in \mathcal{L}_c(\mathbf{A}) \quad (44)$$

where $\mathbf{K} = \bar{\mathbf{C}} + \mathbf{F}$, \mathbf{F} is the regularization matrix defined as $\mathbf{F} = \rho(2\mathbf{I} - \mathbf{1}\mathbf{1}^\top)$, \mathbf{A} is the connectivity matrix, and the set of constraints $\mathcal{L}_c(\mathbf{A})$ restricts \mathbf{L} to a combinatorial graph Laplacian matrix. Considering the graph connectivity is unknown, \mathbf{A} is set to represent a fully connected graph, *i.e.*, $\mathbf{A} = \mathbf{1}\mathbf{1}^\top - \mathbf{I}$. See [63] for details.

We compared our proposed method with several existing EDF graph sampling methods—SP [7], LO [9], NS [8], GDAS [10], and AGBS [13]—for positive and signed graphs constructed from each dataset. Though SP, LO, NS, and GDA were designed and tested for positive graphs without self-loops, we found experimentally that SP, LO, and NS methods can operate for signed graphs also. Thus, we tested those methods using both positive and signed graphs constructed from each dataset.

¹⁰<https://www.ourcommons.ca/members/en/votes>

¹¹<https://www.congress.gov/roll-call-votes>

¹²<https://www.goodcarbadcar.net/2021-canada-automotive-sales/>

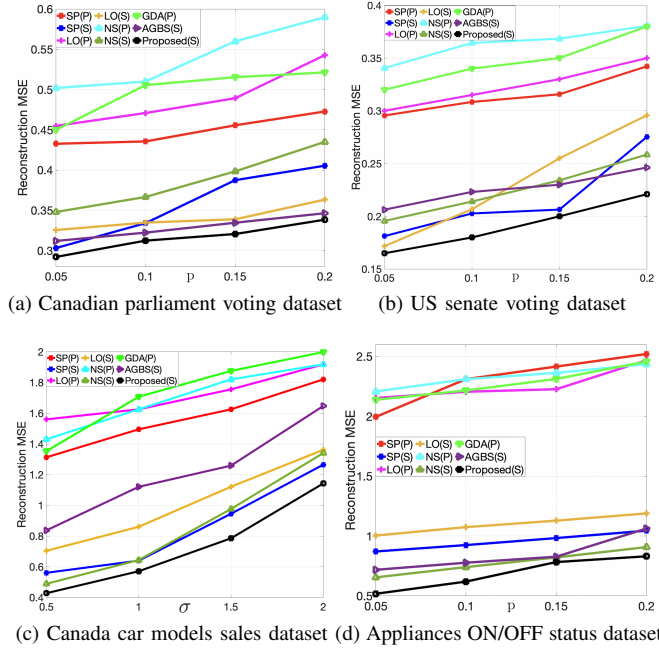


Figure 11. Reconstruction MSE for different sampling algorithms under different noise levels. “P” and “S” within each bracket represent the positive graph and signed graph, respectively.

B. Experimental Results with Different Sampling Budgets

In this experiment, we first employed our proposed and existing sampling methods to each graph constructed from the aforementioned datasets under different sampling budgets. Each method computed a sampling matrix \mathbf{H} for a given sampling budget M . Given a chosen sampling matrix \mathbf{H} , we solved (24) to reconstruct the target signal. Performance of different sampling methods are shown in Fig 10 in terms of signal reconstruction MSE. We observe that the performance of our proposed method is at least as good as the competing schemes at all sampling budgets, and noticeably better when the sampling budgets were small. For example, for the Canadian dataset, our scheme reduced the lowest MSE among competitor schemes by 22.2%, 18.2%, 13.5% and 10.4%, for sampling budget 10, 20, 30 and 40, respectively.

As discussed in Section VIII-A, there exist strong anti-correlations between nodes in all four graphs constructed from these datasets. Thus, a signed graph with both positive and negative edge weights was the most appropriate for each dataset. Thus, as shown in Fig. 10(a), (b), (c) and (d), graph sampling methods using a signed graph (*i.e.*, SP(S), NS(S), LO(S), AGBS(S), Proposed) provided better results than using positive graphs (*i.e.* SP(P), NS(P), LO(P), GDAS(P)).

C. Results with Different Noise Levels

To demonstrate the robustness of our algorithm at different noise levels, we created noisy graph signals as follows.

For test signals from the voting datasets and the appliance ON/OFF status dataset, we added noise so that a signal value can be changed from one value to another with probability $p = 0.05, 0.1, 0.15, 0.2$. For example, in a voting dataset, there are three possible values for any signal entry x_i , *i.e.*, 1, 0, -1 . Assume $x_i = 0$. Then the probability of changing the value of

x_i to 1 or -1 is p . Further, for the car model sales dataset, we added zero mean iid Gaussian noise with standard deviation $\sigma = 0.5, 1, 1.5, 2.0$. For a given noise level (p or σ), we added 100 different noise for each signal, resulting in $100n$ noisy signals for this experiment, where n is the number of original test signals.

Graph sampling performance under different noise levels are shown in Fig 11 in terms of signal reconstruction MSE for the lowest sampling budget used in Fig. 10. For all datasets, we observe that the performance of our proposed method is noticeably better at each noise level. For example, for the US dataset, our proposed method reduced the lowest MSE among competitor methods by 4.1%, 11.3%, 3.1% and 10.2% for noise level $p = 0.05, 0.1, 0.15$ and 0.2, respectively.

IX. CONCLUSION

To model a dataset with inherent anti-correlations, a signed graph with both positive and negative edges is the most appropriate. In this paper, we proposed a fast graph sampling method for signed graphs centered around the concept of *balanced signed graphs* [15]. We first show that balanced signed graphs have a natural notion of graph frequencies based on eigenvectors of the generalized Laplacian matrix [46]. Our graph frequency notion leads to more interpretable low-pass (LP) filter systems for MAP formulated problems regularized with graph smoothness priors. We then design a fast sampling strategy for balanced signed graphs minimizing the LP filter reconstruction error: first balance a graph computed from data using GLASSO [16] via edge weight augmentation, then align Gershgorin disc left-ends via the Gershgorin disc perfect alignment (GDPA) theorem [19]. Finally, a previous sampling algorithm Gershgorin disc alignment sampling (GDAS) [10] is employed. Experiments on four different datasets show that our signed graph sampling method outperformed existing eigen-decomposition-free (EDF) sampling schemes that were designed and tested for positive graphs only.

REFERENCES

- [1] A. Ortega, P. Frossard, J. Kovacevic, J. M. F. Moura, and P. Vандергейст, “Graph signal processing: Overview, challenges, and applications,” *Proc. IEEE*, vol. 106, no. 5, pp. 808–828, May 2018.
- [2] G. Cheung, E. Magli, Y. Tanaka, and M. Ng, “Graph spectral image processing,” *Proc. IEEE*, vol. 106, no. 5, pp. 907–930, May 2018.
- [3] W. Hu, G. Cheung, A. Ortega, and O. Au, “Multi-resolution graph Fourier transform for compression of piecewise smooth images,” *IEEE Trans. Image Process.*, vol. 24, no. 1, pp. 419–433, January 2015.
- [4] J. Pang and G. Cheung, “Graph Laplacian regularization for image denoising: Analysis in the continuous domain,” *IEEE Trans. Image Process.*, vol. 26, no. 4, pp. 1770–1785, 2017.
- [5] X. Liu, G. Cheung, X. Wu, and D. Zhao, “Random walk graph laplacian based smoothness prior for soft decoding of JPEG images,” *IEEE Trans. Image Process.*, vol. 26, no. 2, pp. 509–524, February 2017.
- [6] Y. Tanaka, Y. C. Eldar, A. Ortega, and G. Cheung, “Sampling signals on graphs: From theory to applications,” *IEEE Signal Process. Mag.*, vol. 37, no. 6, pp. 14–30, 2020.
- [7] A. Anis, A. Gadde, and A. Ortega, “Efficient sampling set selection for bandlimited graph signals using graph spectral proxies,” *IEEE Trans. Signal Process.*, vol. 64, no. 14, pp. 3775–3789, 2016.
- [8] F. Wang, G. Cheung, and Y. Wang, “Low-complexity graph sampling with noise and signal reconstruction via neumann series,” *IEEE Trans. Signal Process.*, vol. 67, no. 21, pp. 5511–5526, 2019.
- [9] A. Sakiyama, Y. Tanaka, T. Tanaka, and A. Ortega, “Eigendecomposition-free sampling set selection for graph signals,” *IEEE Trans. Signal Process.*, vol. 67, no. 10, pp. 2679–2692, 2019.

[10] Y. Bai, F. Wang, G. Cheung, Y. Nakatsukasa, and W. Gao, "Fast graph sampling set selection using Gershgorin disc alignment," *IEEE Trans. Signal Process.*, vol. 68, pp. 2419–2434, 2020.

[11] W. T. Su, G. Cheung, and C. W. Lin, "Graph fourier transform with negative edges for depth image coding," in *ICIP*, 2017, pp. 1682–1686.

[12] G. Cheung, W. T. Su, Y. Mao, and C. W. Lin, "Robust semisupervised graph classifier learning with negative edge weights," *IEEE Trans. Signal Inf. Process. Netw.*, vol. 4, no. 4, pp. 712–726, 2018.

[13] C. Dinesh, G. Cheung, F. Wang, and I. V. Bajic, "Sampling of 3D point cloud via gershgorin disc alignment," in *ICIP*, 2020.

[14] C. Dinesh, G. Cheung, and I. V. Bajic, "Point cloud sampling via graph balancing and Gershgorin disc alignment," *IEEE Trans. Pattern Anal. Mach. Intell.*, pp. 1–1, 2022.

[15] D. Easley and J. Kleinberg, *Networks, crowds, and markets: Reasoning about a Highly Connected World*, vol. 8, Cambridge university press Cambridge, 2010.

[16] J. Friedman, T. Hastie, and R. Tibshirani, "Sparse inverse covariance estimation with the graphical lasso," *Biostatistics (Oxford, England)*, vol. 9, pp. 432–41, 08 2008.

[17] J. Pang and G. Cheung, "Graph Laplacian regularization for inverse imaging: Analysis in the continuous domain," *IEEE Trans. Image Process.*, vol. 26, no.4, pp. 1770–1785, April 2017.

[18] R. S. Varga, *Gershgorin and his circles*, Springer, 2004.

[19] C. Yang, G. Cheung, and W. Hu, "Signed graph metric learning via gershgorin disc perfect alignment," *IEEE Trans. Pattern Anal. Mach. Intell.*, pp. 1–1, 2021.

[20] A. G. Marques, S. Segarra, G. Leus, and A. Ribeiro, "Sampling of graph signals with successive local aggregations," *IEEE Trans. Signal Process.*, vol. 64, no. 7, pp. 1832–1843, 2016.

[21] D. Valsesia, G. Fracastoro, and E. Magli, "Sampling of graph signals via randomized local aggregations," *IEEE Trans. Signal Inf. Process. Netw.*, vol. 5, no. 2, pp. 348–359, 2019.

[22] X. Wang, J. Chen, and Y. Gu, "Local measurement and reconstruction for noisy bandlimited graph signals," *Signal Processing*, vol. 129, pp. 119–129, 2016.

[23] I. Pesenson, "Sampling in paley-wiener spaces on combinatorial graphs," *Transactions of the American Mathematical Society*, vol. 360, no. 10, pp. 5603–5627, 2008.

[24] S. Chen, R. Varma, A. Sandryhaila, and J. Kovacevic, "Discrete signal processing on graphs: Sampling theory," *IEEE Trans. Signal Process.*, vol. 63, no. 24, pp. 6510–6523, 2015.

[25] F. Wang, Y. Wang, and G. Cheung, "A-optimal sampling and robust reconstruction for graph signals via truncated Neumann series," in *IEEE Signal Process. Lett.*, May 2018, vol. 25, no.5, pp. 680–684.

[26] H. Shomorony and A.S. Avestimehr, "Sampling large data on graphs," in *IEEE GlobalSIP*, 2014, pp. 933–936.

[27] G. Puy, N. Tremblay, R. Gribonval, and P. Vandergheynst, "Random sampling of bandlimited signals on graphs," *Applied and Computational Harmonic Analysis*, vol. 44, no. 2, pp. 446–475, 2018.

[28] G. Ortiz-Jiménez, M. Coutino, S. P. Chepuri, and G. Leus, "Sampling and reconstruction of signals on product graphs," in *IEEE GlobalSIP*, 2018, pp. 713–717.

[29] G. Puy and P. Pérez, "Structured sampling and fast reconstruction of smooth graph signals," *Information and Inference: A Journal of the IMA*, vol. 7, no. 4, pp. 657–688, 2018.

[30] M. Tsitsvero, S. Barbarossa, and P. Di Lorenzo, "Signals on graphs: Uncertainty principle and sampling," *IEEE Trans. Signal Process.*, vol. 64, no. 18, pp. 4845–4860, 2016.

[31] L. F. Chamom and A. Ribeiro, "Greedy sampling of graph signals," *IEEE Trans. Signal Process.*, vol. 66, no. 1, pp. 34–47, 2017.

[32] F. Pukelsheim, *Optimal design of experiments*, SIAM, 2006.

[33] A. Sakiyama, Y. Tanaka, T. Tanaka, and A. Ortega, "Accelerated sensor position selection using graph localization operator," in *IEEE ICASSP*, 2017, pp. 5890–5894.

[34] D. K. Hammond, P. Vandergheynst, and R. Gribonval, "Wavelets on graphs via spectral graph theory," *Applied and Computational Harmonic Analysis*, vol. 30, no. 2, pp. 129–150, 2011.

[35] C. Dinesh, S. Bagheri, G. Cheung, and I. V. Bajic, "Linear-time sampling on signed graphs via Gershgorin disc perfect alignment," in *IEEE ICASSP*, 2022, pp. 5942–5946.

[36] S. Chen, A. Sandryhaila, J. Moura, and J. Kovacevic, "Signal recovery on graphs: Variation minimization," in *IEEE Trans. Signal Process.*, September 2015, vol. 63, no.17, pp. 4609–4624.

[37] A. Elmoataz, O. Lezoray, and S. Bougleux, "Nonlocal discrete regularization on weighted graphs: a framework for image and manifold processing," *IEEE Trans. Image Process.*, vol. 17, no. 7, pp. 1047–1060, 2008.

[38] C. Couprise, L. Grady, L. Najman, J. C. Pesquet, and H. Talbot, "Dual constrained TV-based regularization on graphs," *SIAM Journal on Imaging Sciences*, vol. 6, no. 3, pp. 1246–1273, 2013.

[39] F. Chen, G. Cheung, and X. Zhang, "Manifold graph signal restoration using gradient graph laplacian regularizer," *arXiv preprint arXiv:2206.04245*, 2022.

[40] A. Ortega, *Introduction to graph signal processing*, Cambridge University Press, 2022.

[41] D. I. Shuman, S. K. Narang, P. Frossard, A. Ortega, and P. Vandergheynst, "The emerging field of signal processing on graphs: Extending high-dimensional data analysis to networks and other irregular domains," *IEEE Signal Process. Mag.*, vol. 30, no. 3, pp. 83–98, 2013.

[42] V. N. Ekambaram, G. C. Fanti, B. Ayazifar, and K. Ramchandran, "Multiresolution graph signal processing via circulant structures," in *IEEE Digital Signal Processing and Signal Processing Education Meeting*, 2013, pp. 112–117.

[43] X. Zhu and M. Rabbat, "Approximating signals supported on graphs," in *IEEE ICASSP*, 2012, pp. 3921–3924.

[44] A. Sandryhaila and J. M. F. Moura, "Discrete signal processing on graphs," *IEEE Trans. Signal Process.*, vol. 61, no. 7, pp. 1644–1656, 2013.

[45] A. Sandryhaila and J. M. F. Moura, "Discrete signal processing on graphs: Frequency analysis," *IEEE Trans. Signal Process.*, vol. 62, no. 12, pp. 3042–3054, 2014.

[46] T. Biyikoglu, J. Leydold, and P. F. Stadler, "Nodal domain theorems and bipartite subgraphs," *The Electronic Journal of Linear Algebra*, vol. 13, pp. 344–351, 2005.

[47] G. Strang, "The discrete cosine transform," *SIAM review*, vol. 41, no. 1, pp. 135–147, 1999.

[48] J. Leskovec, D. Huttenlocher, and J. Kleinberg, "Signed networks in social media," in *Proceedings of the SIGCHI conference on human factors in computing systems*, 2010, pp. 1361–1370.

[49] C. I. Connolly and R. A. Grupen, "The applications of harmonic functions to robotics," *Journal of robotic Systems*, vol. 10, no. 7, pp. 931–946, 1993.

[50] R. Mazumder and T. Hastie, "The graphical lasso: New insights and alternatives," *Electron. J. Statist.*, vol. 6, pp. 2125–2149, 2012.

[51] E. Brian Davies, Josef Leydold, and Peter F. Stadler, "Discrete nodal domain theorems," *Elsevier Linear Algebra and its Application*, 2000.

[52] R. A. Horn and C. R. Johnson, *Matrix analysis*, Cambridge university press, 2012.

[53] H. Rue and L. Held, *Gaussian Markov random fields: theory and applications*, CRC press, 2005.

[54] K. J. Merikoski and R. Kumar, "Inequalities for spreads of matrix sums and products," *Applied Mathematics E-Notes*, vol. 4, pp. 150–159, 2004.

[55] L. F. O. Chamom and A. Ribeiro, "Greedy sampling of graph signals," *IEEE Trans. Signal Process.*, vol. 66, no. 1, pp. 34–47, 2018.

[56] R. S. Varga, *Gershgorin and his circles*, vol. 36, Springer Science & Business Media, 2010.

[57] Y. Bai, G. Cheung, F. Wang, X. Liu, and W. Gao, "Reconstruction-cognizant graph sampling using gershgorin disc alignment," in *ICASSP*, 2019, pp. 5396–5400.

[58] M. Milgram, "Irreducible graphs," *Journal of Combinatorial Theory, Series B*, vol. 12, no. 1, pp. 6–31, 1972.

[59] A. V. Knyazev, "Toward the optimal preconditioned eigensolver: Locally optimal block preconditioned conjugate gradient method," *SIAM journal on scientific computing*, vol. 23, no. 2, pp. 517–541, 2001.

[60] R. A. Horn and C. R. Johnson, *Matrix analysis*, Cambridge university press, 1990.

[61] J. Zeng, G. Cheung, and A. Ortega, "Bipartite approximation for graph wavelet signal decomposition," *IEEE Trans. Signal Process.*, vol. 65, no. 20, pp. 5466–5480, Oct 2017.

[62] S. Makonin, B. Ellert, I. Bajic, and F. Popowich, "Electricity, water, and natural gas consumption of a residential house in canada from 2012 to 2014," *Scientific Data*, vol. 3, pp. 1–12, 2016.

[63] H. E. Egilmez, E. Pavez, and A. Ortega, "Graph learning from data under laplacian and structural constraints," *IEEE J. Sel. Topics Signal Process.*, vol. 11, no. 6, pp. 825–841, Sep. 2017.